

TE-Wave Propagation over an Impedance-Matched RHM to LHM Transition in a Hollow Waveguide

Balwan Rana^{*}, Brage B. Svendsen, and Mariana Dalarsson

Abstract—We study TE-wave propagation in a hollow waveguide with a graded transition from a lossy right-handed material (RHM) filling the left-hand half of the waveguide to the impedance-matched lossy left-handed material (LHM) filling the right-hand half of the waveguide. The transition between the two media is graded along the direction perpendicular to the boundary between the two materials (chosen to be the z -direction), and the permittivity $\varepsilon(\omega, z)$ and permeability $\mu(\omega, z)$ are chosen to vary according to hyperbolic tangent functions along the z -direction. We obtain exact analytical solutions to Maxwell's equations for lossy media, and the solutions for the field components confirm the expected properties of RHM-LHM structures. Thereafter, a numerical study of the wave propagation over an impedance-matched graded RHM-LHM interface is performed, using COMSOL software. The numerical study shows an excellent agreement between the numerical simulations and analytical results. Compared to other solution methods, the present approach has the advantage of being able to model more realistic smooth transitions between different materials. However, in the limiting case, it includes correct results for abrupt transitions as well. In the present approach we also introduce interface width as an additional degree of freedom that can be used in the design of practical RHM-LHM interfaces.

1. INTRODUCTION

In the present paper, we study graded material composites consisting of right-handed materials (RHM) and left-handed materials (LHM), with permittivities and permeabilities being continuous functions of the spatial coordinates. Such composites, with spatially varying permittivities and permeabilities are of interest in a number of current state-of-the-art research areas, and are given an increasing theoretical and experimental attention over the last two decades.

Transformation optics (TO) [1] is one major area of interest, with the creation of novel optical devices, such as waveguide adapters, waveguide crossings and light source collimators. TO-based applications have shown remarkable design flexibility due to the introduction of spatially varying electric and magnetic material properties. The exceptional optical performance and efficient on-chip integrability of the abovementioned devices is numerically confirmed in [1]. These specific TO-based designs use materials with spatially-varying dielectric material properties only, and there is no need of spatially varying magnetic material properties. Thus they can be used in integrated, broadband and low-loss photonic applications.

TO is useful in a number of other applications including specialized antennas [2, 3], hyperlens applications [4, 5], and subwavelength images [6, 7]. In [2], an impedance-matched gradient refractive index (GRIN) based lens antenna is studied. The designed antenna [2] is composed of metamaterials that are inhomogeneous but isotropic and can provide impedance-matching to the free space. It is shown that such an approach can enable compact and high-performance antenna designs. In [3],

Received 25 February 2022, Accepted 24 March 2022, Scheduled 18 April 2022

^{*} Corresponding author: Balwan Rana (balwan@kth.se).

The authors are with Department of Electrical Engineering, School of Electrical Engineering and Computer Science, KTH Royal Institute of Technology, 100 44 Stockholm, Sweden.

the authors present a flat high-gain TO GRIN-lens antenna with beam scanning capability and dual-polarization. The presented design is useful for far-field imaging, remote sensing, multi-beam steering and scanning. In [4], a profiled lens-assisted spot size converter has been demonstrated to provide an excellent combination of both a reduced footprint and lower insertion losses. The GRIN-lens-assisted spot size converter has also shown to allow for a larger bandwidth and a higher tolerance to fabrication errors, thereby displaying the possibility of an ultra-compact, robust, and efficient spot size converter with a GRIN profile. In the article written by Gauffillet et al. [5], the GRIN metamaterials are shown to be suitable for designing photonic components (metadevices) for applications at THz frequencies. The study in question made use of a dielectric metamaterial-based GRIN lens in the THz frequency range. Utilizing the capability of metamaterials to convert evanescent waves to propagating waves, Salami et al. [6] studied far-field subwavelength imaging using phase-gradient metasurfaces. In [7], similar principles are used for far-field nanorod superlenses in biological media.

The phenomenon of electromagnetic cloaking is another area, where TO principles in metamaterial composites with spatially varying electric and magnetic material properties are of major interest. Such composites offer the possibility to manipulate surface waves in THz and optical frequency ranges. As an example, in [8], it has been experimentally demonstrated how a surface wave cloak can be obtained using artificial GRIN materials with nanocomposites that control surface wave propagation.

For the present study, waveguide applications [9,10] are of particular interest. For example in [11], it is shown numerically that a nanostructured waveguide design, with a tunable absorption spectrum, can enhance the performance of solar cells.

Another area of interest concerns light trapping in waveguides [12,13]. In [12] a graded metamaterial waveguide is used to trap and release light in the mid-infrared frequency range. In [13], an improved theoretical structure for trapped storage of light has been proposed using a hyperbolic tangent graded metamaterial. The light-trapping characteristics discussed in [12] and [13] propose a graded metamaterial waveguide to be a prime candidate for multi-wavelength absorption, optical modulation, switching, communication and other light-matter interactions.

Yet another area of interest concerns the minimization and customization of waveguides [14,15]. In [14] a proposed meta-waveguide structure and a derived transcendental equation has been used to reveal the physical mechanisms behind phase control of metamaterial waveguides. The results show that waveguides filled with a graded-index metamaterial allow for customizing phase modulation and absorption in the microwave frequency region. In [15], a semi-analytical method is proposed to calculate the eigenvalues, including the cutoff wavenumbers and dispersion relations, for waveguides filled with GRIN metamaterials. This method is based on modal expansion analysis, and has been shown to highlight the observed below-cutoff backward wave propagation phenomenon in waveguides filled with GRIN metamaterials.

Related to the area of minimization and customization of waveguides, it has been shown [16] that it is possible to fabricate low-loss glass-ceramics waveguides activated by rare-earth ions, which opens the possibility to develop cheap and smart integrated optical circuits. Another issue of interest is the possibility of realizing magnetic-free non-reciprocity [17,18] of waveguides and other optical devices.

Another area of interest is topological metamaterials, which can significantly improve the performance of novel microwave devices. Topological metamaterials have been shown to possess a high compatibility with novel microwave and circuit devices, such as phased antenna arrays and traveling-wave amplifiers [19]. The advantages of such designs include inherent protection and reduced sensitivity to structural imperfections. In [20], a passive S-band triplexer is designed using complementary split ring resonators (CSRRs) and an interdigital capacitor. Such a design has low insertion loss, channel isolation and fractional bandwidth compared to novel passive S-band triplexers. In [21], a four-port compact active duplexer based on a CSRR and interdigital loaded microstrip coupled lines (CSRR-IL MCL) is studied. The design has a high amplification, low return loss and fractional bandwidth. The collection of works [19–21] show that topological metamaterials in novel microwave devices could affect the performance of these devices significantly. This suggests that further analytical, numerical, and experimental studies of metamaterial composites are necessary in order to determine the limits to their performance and capabilities.

Due to their unprecedented performance and unique applicability, there is an increasing interest in both analytical and numerical studies of GRIN metamaterial composites with impedance matching in

contemporary electromagnetic research. Following the approach employed in [22–25], in this paper we consider a new problem of TE-wave propagation over an impedance-matched RHM to LHM transition in a hollow waveguide. The complete analytical solutions for the fields, including the well-known transverse functions, will be written out for the particular example of rectangular waveguide. It should however be noted that the our results are valid for hollow waveguides of arbitrary cross-sections (e.g., cylindrical, coaxial, elliptical cross-sections), as long as the analytical solutions for the transverse functions for such waveguides are available.

At this point, it is important to highlight the fundamental difference between the research in the present paper, and the previous research reported in [22–25] and a few other earlier publications by one of the present authors (M. Dalarsson). Firstly, the previous research reported in [22–24] dealt with plane wave propagation in unbound media, not confined in any waveguide structures. The results in [22–24] are theoretically important and a good first step to a full understanding of the wave-propagation in graded RHM-LHM composites. However, in most practical applications, material composites cannot be described as unbound media. Thus, the results obtained in [22–24] cannot be readily applied to analyze most of the aforementioned practical devices. It is therefore of importance to generalize these studies to that of wave propagation in RHM-LHM composites confined in hollow waveguides.

The results for wave propagation in RHM-LHM material composites confined in hollow waveguides were, to the best of our knowledge, never reported before the paper [25]. Although the mathematical equations describing the two physical situations may at a first glance appear similar to each other, the solutions are fundamentally different. The solutions obtained in the present paper are considerably more mathematically complex and require different mathematical solution techniques.

Secondly, while the work in [25] also describes TE-wave propagation in a graded material composite confined in a hollow waveguide, the research question in that paper is very different from that of the present paper. The graded material composite in [25] was a model of a non-magnetic biological tissue with and without gold nanoparticles (GNPs) in a study aiming to create knowledge about energy absorption in GNP-substrates inserted in a waveguide. The entire material composite studied in [25] consists of two different RHM media, and there are no artificial LHM materials involved at all. The mathematical equations describing TE-wave propagation through such a graded RHM composite are fundamentally different from those described in the present paper. The results for the fields are also very different and require different mathematical solution techniques.

In conclusion, it is important to note that we intentionally try to keep the notation consistent with all our previous work (e.g., [22–25]), in order to identify potential mathematical and practical synergies between different studies. By doing so, it is sometimes possible to facilitate new mathematical solutions and identify new potential interdisciplinary applications for our work, like in [25]. However, that does not imply any significant similarity between the different physical situations investigated.

2. PROBLEM DESCRIPTION

The geometry of the problem consists of a hollow waveguide with graded transition from a lossy RHM filling the left-hand half of the waveguide to the impedance-matched lossy LHM filling the right-hand half of the waveguide, as shown in Figure 1(a). The cross-section of the rectangular waveguide, used as an example in the present paper, is shown in Figure 1(b). In addition, an illustration of the hyperbolic tangent function behaviour of the real parts of material parameters (permittivity and permeability) is displayed in Figure 1(c).

Using the $\exp(i\omega t)$ time convention, we define the permittivity and permeability in the entire waveguide structure as continuous functions given by

$$\varepsilon(\omega, z) = -\varepsilon_0 \frac{\varepsilon_{I1} + \varepsilon_{I2}}{2\beta} \left(\tanh \frac{z}{z_0} + i\beta \right) \quad , \quad \mu(\omega, z) = -\mu_0 \frac{\mu_{I1} + \mu_{I2}}{2\beta} \left(\tanh \frac{z}{z_0} + i\beta \right) \quad (1)$$

where ε_0 and μ_0 are the permittivity and permeability of free space, respectively; z_0 is a measure of the length of the transition region between the two materials; and β is the loss parameter defined in [22], given in Eq. (2) below. In Eq. (1), $\varepsilon_1(\omega) = \varepsilon_0[+\varepsilon_R(\omega) - i\varepsilon_{I1}(\omega)]$ and $\mu_1(\omega) = \mu_0[+\mu_R(\omega) - i\mu_{I1}(\omega)]$ are the spatially constant dispersive complex permittivity and permeability of the RHM medium, respectively. For the RHM medium, $\varepsilon_R(\omega)$ and $\mu_R(\omega)$ are the positive real parts of the relative

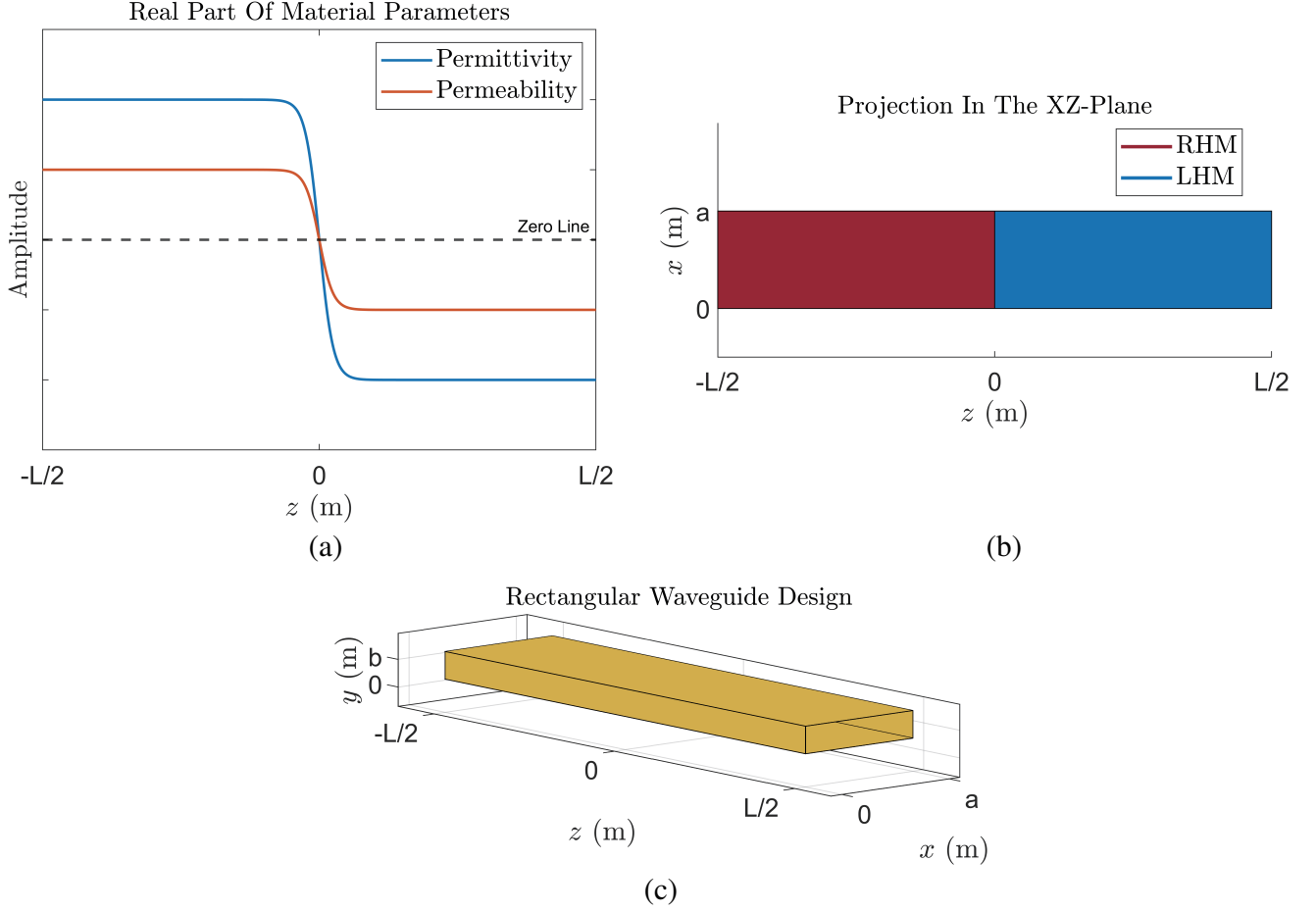


Figure 1. (a) Waveguide with RHM-LHM transition. (b) Rectangular waveguide example. (c) Hyperbolic tangent function behaviour of the real parts of material permittivity and permeability.

permittivity and permeability, respectively, while $-\varepsilon_{I1}(\omega)$ and $-\mu_{I1}(\omega)$ are the negative imaginary parts of the relative permittivity and relative permeability, respectively. Similarly $\varepsilon_2(\omega) = \varepsilon_0[-\varepsilon_R(\omega) - i\varepsilon_{I2}(\omega)]$ and $\mu_2(\omega) = \mu_0[-\mu_R(\omega) - i\mu_{I2}(\omega)]$ are the spatially constant dispersive complex permittivity and permeability of the LHM medium, respectively. For the LHM medium, $-\varepsilon_R(\omega)$ and $-\mu_R(\omega)$ are the negative real parts of the relative permittivity and permeability, respectively, while $-\varepsilon_{I2}(\omega)$ and $-\mu_{I2}(\omega)$ are the negative imaginary parts of the relative permittivity and relative permeability, respectively. Here we recall from, e.g., [22], that the impedance-matching condition requires that

$$\beta = \frac{\varepsilon_{I1} + \varepsilon_{I2}}{2\varepsilon_R - i(\varepsilon_{I1} - \varepsilon_{I2})} = \frac{\mu_{I1} + \mu_{I2}}{2\mu_R - i(\mu_{I1} - \mu_{I2})} \quad (2)$$

Asymptotically, for $z \rightarrow -\infty$, in the RHM material we have $\varepsilon_1(\omega, z) = \varepsilon_0(\varepsilon_R - i\varepsilon_{I1})$ and $\mu_1(\omega, z) = \mu_0(\mu_R - i\mu_{I1})$. In the LHM material asymptotically, for $z \rightarrow +\infty$, we have $\varepsilon_2(\omega, z) = \varepsilon_0(-\varepsilon_R - i\varepsilon_{I2})$ and $\mu_2(\omega, z) = \mu_0(-\mu_R - i\mu_{I2})$, as required by impedance matching in passive materials. The wave equation for the transverse electric field $\mathbf{E}(x, y, z)$ (TE waves have $E_z = 0$) is given by

$$\nabla^2 \mathbf{E} - \frac{1}{\mu} \frac{d\mu}{dz} \frac{\partial \mathbf{E}}{\partial z} + \omega^2 \varepsilon \mu \mathbf{E} = 0 \quad , \quad \mathbf{E} = \mathbf{E}_T = E_x \hat{x} + E_y \hat{y} \quad (3)$$

The corresponding wave equation for the magnetic field \mathbf{H} is not needed, since the magnetic field can be obtained directly from Maxwell's equation $\nabla \mathbf{E} = -i\omega\mu(z)\mathbf{H}$. The approach to solve the wave equation (3) is based on variable separation such that $\mathbf{E}(x, y, z) = \mathbf{T}(x, y)L(z)$, where the transverse vector

$\mathbf{T}(x, y)$ and the longitudinal function $L(z)$ satisfy following equations

$$\nabla_t^2 \mathbf{T} + k_t^2 \mathbf{T} = \left(\frac{\partial^2}{\partial x^2} + \frac{\partial^2}{\partial y^2} \right) \mathbf{T} + k_t^2 \mathbf{T} = 0 \quad , \quad \frac{d^2 L}{dz^2} - \frac{1}{\mu} \frac{d\mu}{dz} \frac{dL}{dz} + k_z^2(z)L = 0 \quad (4)$$

Here, the square of the spatially dependent wave vector is given by $k^2(z) = \omega^2 \varepsilon(z) \mu(z)$, such that in the case of rectangular waveguide shown in Figure 1(b), we can write down the squares of the transverse (k_t^2) and longitudinal (k_z^2) components of the wave vector in the form

$$k_t^2 = \left(\frac{m\pi}{a} \right)^2 + \left(\frac{n\pi}{b} \right)^2 \quad , \quad k_z^2(z) = \omega^2 \varepsilon(z) \mu(z) - k_t^2 = k^2(z) - k_t^2 \quad (5)$$

3. SOLUTIONS FOR THE FIELDS

Here we note that the transverse parts of the solutions, satisfying the correct boundary conditions, are not affected by the z -dependence of material parameters $\varepsilon(\omega, z)$ and $\mu(\omega, z)$. Thus, they have the well-known textbook form

$$T_x(x, y) \propto \left(\frac{n\pi}{b} \right) \cos \left(\frac{m\pi}{a} x \right) \sin \left(\frac{n\pi}{b} y \right) \quad (6)$$

$$T_y(x, y) \propto \left(\frac{m\pi}{a} \right) \sin \left(\frac{m\pi}{a} x \right) \cos \left(\frac{n\pi}{b} y \right) \quad (7)$$

By the above separation of variables with $L(z) = \mu(z)Z(z)$, we obtain the solutions for the electric field components for the case of TE-wave propagation in a rectangular waveguide with graded transition from a lossy RHM material filling the left-hand half of the waveguide to the impedance-matched lossy LHM material filling the right-hand half of the waveguide in the following form

$$E_x(\mathbf{r}) = \frac{i\omega\mu(z)}{k_t^2} \left(\frac{n\pi}{b} \right) H_0 \cos \left(\frac{m\pi}{a} x \right) \sin \left(\frac{n\pi}{b} y \right) Z(z) \quad (8)$$

$$E_y(\mathbf{r}) = -\frac{i\omega\mu(z)}{k_t^2} \left(\frac{m\pi}{a} \right) H_0 \sin \left(\frac{m\pi}{a} x \right) \cos \left(\frac{n\pi}{b} y \right) Z(z) \quad (9)$$

In Eqs. (6) and (7), a and b ($a > b$) are the waveguide dimensions shown in Figure 1(b). The longitudinal function $Z(z)$ is obtained in the following form

$$Z(z) = \exp \left[-i \int k_z(z) dz \right] = \exp \left[-i \int \sqrt{\omega^2 \varepsilon(z) \mu(z) - k_t^2} dz \right] \quad (10)$$

where we readily see that $Z'(z) = -ik_z(z)Z(z)$. Furthermore, we note that for constant ε and μ , we obtain $Z(z) = \exp(-ik_z z)$, as required. When we know the solutions for the two components of the electric field, we readily obtain the longitudinal magnetic field component H_z by direct application of the Maxwell's equation

$$\mathbf{H} = \frac{i}{\omega\mu(z)} \nabla \times \mathbf{E} \Rightarrow H_z(\mathbf{r}) = \frac{i}{\omega\mu(z)} \left(\frac{\partial E_y}{\partial x} - \frac{\partial E_x}{\partial y} \right) = H_0 \cos \left(\frac{m\pi}{a} x \right) \cos \left(\frac{n\pi}{b} y \right) Z(z) \quad (11)$$

Using Eq. (11), we further obtain the two transverse magnetic field components, as follows

$$H_x(\mathbf{r}) = -\frac{i}{\omega\mu(z)} \frac{\partial E_y}{\partial z} = -\frac{1}{k_t^2} \left[\frac{1}{\mu} \frac{d\mu}{dz} - ik_z(z) \right] \left(\frac{m\pi}{a} \right) H_0 \sin \left(\frac{m\pi}{a} x \right) \cos \left(\frac{n\pi}{b} y \right) Z(z) \quad (12)$$

$$H_y(\mathbf{r}) = \frac{i}{\omega\mu(z)} \frac{\partial E_x}{\partial z} = -\frac{1}{k_t^2} \left[\frac{1}{\mu} \frac{d\mu}{dz} - ik_z(z) \right] \left(\frac{n\pi}{b} \right) H_0 \cos \left(\frac{m\pi}{a} x \right) \sin \left(\frac{n\pi}{b} y \right) Z(z) \quad (13)$$

Here we note that for constant μ (such that $d\mu/dz = 0$), the two results in Eqs. (12) and (13) are reduced to the well-known magnetic field components for rectangular waveguides filled with non-graded media.

Introducing the definitions of the material parameters in Eq. (1), the expression (10) for $Z(z)$ can be evaluated as follows

$$\begin{aligned}
Z(z) = & \exp \left(-i \int \sqrt{\kappa^2 \left(\tanh \frac{z}{z_0} + i\beta \right)^2 - k_t^2} dz \right) = \left[\left(\tanh \frac{z}{z_0} + i\beta \right) + \frac{k_z(z)}{\kappa} \right]^{i\kappa z_0} \\
& \cdot \left\{ \left[\exp \left(2 \frac{z}{z_0} \right) + 1 \right] \left[(1 + i\beta) \left(\tanh \frac{z}{z_0} + i\beta \right) - \frac{k_t^2}{\kappa^2} + \frac{k_z(+\infty)k_z(z)}{\kappa^2} \right] \right\}^{-ik_z(+\infty)z_0/2} \\
& \cdot \left\{ \left[\exp \left(-2 \frac{z}{z_0} \right) + 1 \right] \left[(-1 + i\beta) \left(\tanh \frac{z}{z_0} + i\beta \right) - \frac{k_t^2}{\kappa^2} + \frac{k_z(-\infty)k_z(z)}{\kappa^2} \right] \right\}^{ik_z(-\infty)z_0/2} \quad (14)
\end{aligned}$$

where

$$\kappa^2 = \omega^2 \varepsilon_0 \mu_0 \frac{\varepsilon_{I1} + \varepsilon_{I2}}{2\beta} \frac{\mu_{I1} + \mu_{I2}}{2\beta} = \omega^2 \varepsilon_0 \mu_0 \left[\varepsilon_R - i \frac{\varepsilon_{I1} - \varepsilon_{I2}}{2} \right] \left[\mu_R - i \frac{\mu_{I1} - \mu_{I2}}{2} \right] \quad (15)$$

is a complex-valued function of frequency, constant with respect to the integration of the spatial dimension z . The function $Z(z)$ is the graded equivalent of the non-graded z -dependent part of the standard non-graded solution. For non-graded transitions, it is simply equal to $\exp(-ik_z z)$, and its real part is simply an attenuated cosine function. However, for graded transitions, $Z(z)$ represents a more mathematically complex propagating wave in the z -direction in an inhomogeneous composite. It is asymptotically (far from the interface between the two materials, where $z \rightarrow \pm\infty$) equal to $\exp(-ik_z(\pm\infty)z)$, but displays a different behavior about the interface between the two materials ($z = 0$). It should be noted here that $Z(z)$ automatically produces the switch from positive to negative wave-propagation direction when passing from RHM to LHM.

4. NUMERICAL SOLUTIONS AND COMPARISON TO THE ANALYTICAL RESULTS

The finite element method based software COMSOL Multiphysics is used to model a lossy impedance-matched graded interface between RHM and LHM media inside a hollow waveguide. A three-dimensional hyperrectangle is designed to represent the waveguide, with the width $a = 0.5$ m, height $b = 0.1$ m and length $L = 2$ m. The center of the waveguide is placed at the origin. The hollow volume inside the waveguide is occupied by an inhomogeneous RHM-LHM composite modelled according to the analytical functions in Eq. (1) with the impedance-matching condition (2). The hollow waveguide is oriented such that the excited wave travels from negative z -values (the left) to positive z -values (the right). In this design, the RHM occupies the negative z -axis whilst the LHM occupies the positive z -axis. Consequently, the receiving port is placed to the right of the LHM and the exciting port to the left of the RHM. In addition, both the exciting and receiving ports were backed by perfectly matched layers (PMLs). The PML next to the receiving port was scaled by a factor of -1 . This was done in order to ensure proper absorption functionality of the layers when dealing with LHMs. Furthermore, perfect electric conductor (PEC) boundary conditions were applied to the surrounding faces of the waveguide and PMLs. In addition, the scattering boundary condition was applied to the outward facing sides of these layers. The complete implementation was tested in a 2D domain as well as a 3D domain. The results indicate an excellent correspondence to one another with properly chosen mode phases in 2D and 3D models.

In the present section, we present the numerical and analytical results for the electric field intensity $E(x, y, z)$ for the TE₁₀ mode in Figures 2 and 3. In Figure 2, the 2D electric field intensity $E(x = 0, y = 0, z)$ in the middle of the hollow waveguide is shown. Here, we note that subfigures (a) and (b) represent the COMSOL and analytical results, respectively. In subfigures (c) and (d), we present a comparison between the COMSOL and analytical results for real and imaginary parts of the field intensity. In Figure 3, the 3D electric field intensity $E(x, y, z)$ inside the hollow waveguide is displayed. Subfigures (a) and (b) represent the real and imaginary part of the 2D results displayed in Figure 2 respectively. The normalized magnitude of the electric field intensity is displayed on the vertical axis. The gradient transition of the medium permittivity and permeability has a steepness

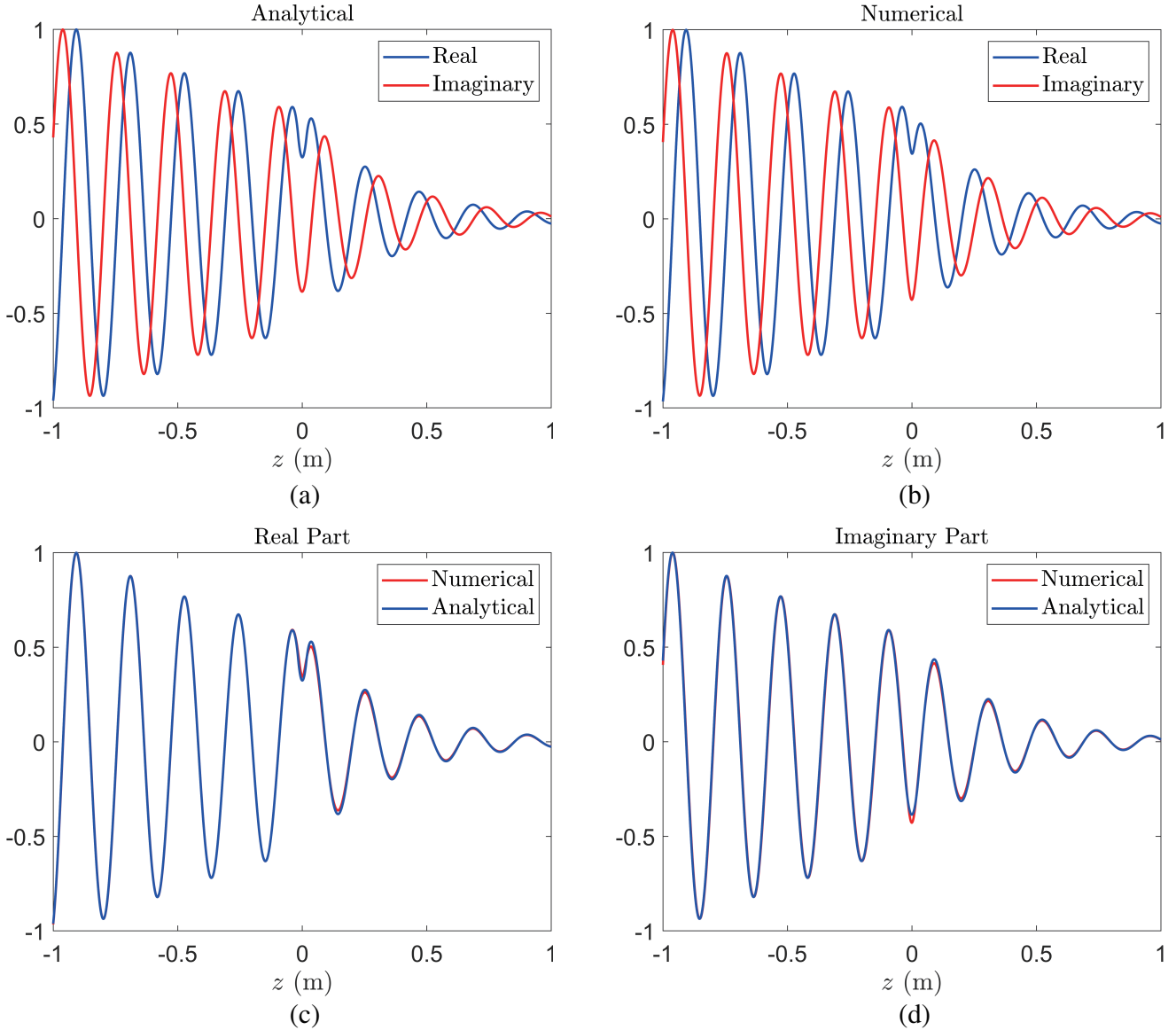


Figure 2. Numerically and analytically obtained results for the TE_{10} electric field intensity $E(x = 0, y = 0, z)$ in the middle of the waveguide. figures (a) and (b) show the numerical and analytical results, respectively, while the figures (c) and (d) show a comparison between the real and imaginary parts of the numerical and analytical electric field intensities, respectively.

factor of $z_0 = 0.01$ m. In addition, the RHM has the material properties $\epsilon = 2 + 0.04i$ and $\mu = 1 + 0.02i$, while the LHM has the material properties $\epsilon = -2 + 0.2i$ and $\mu = -1 + 0.1i$. For this implementation, we have chosen the LHM to be more lossy than the RHM. This has been done in order to model a realistic RHM-LHM composite, where we know that LHM typically has larger losses than RHM. The operational frequency for the simulation is chosen to be 1 GHz.

In Figure 2, we observe an excellent agreement between the analytical and numerical results, confirming the validity of the results. Furthermore, from the real parts of the two-dimensional field intensity functions, we observe the phase change, i.e., the change of the direction of the wave vector at $z = 0$, as required. The behavior of the two-dimensional field intensity functions is similar to the corresponding behavior of the fields in our previous studies [22–24], despite the different nature of the solutions. It indicates that RHM-LHM composites confined in waveguides behave similarly to unbound

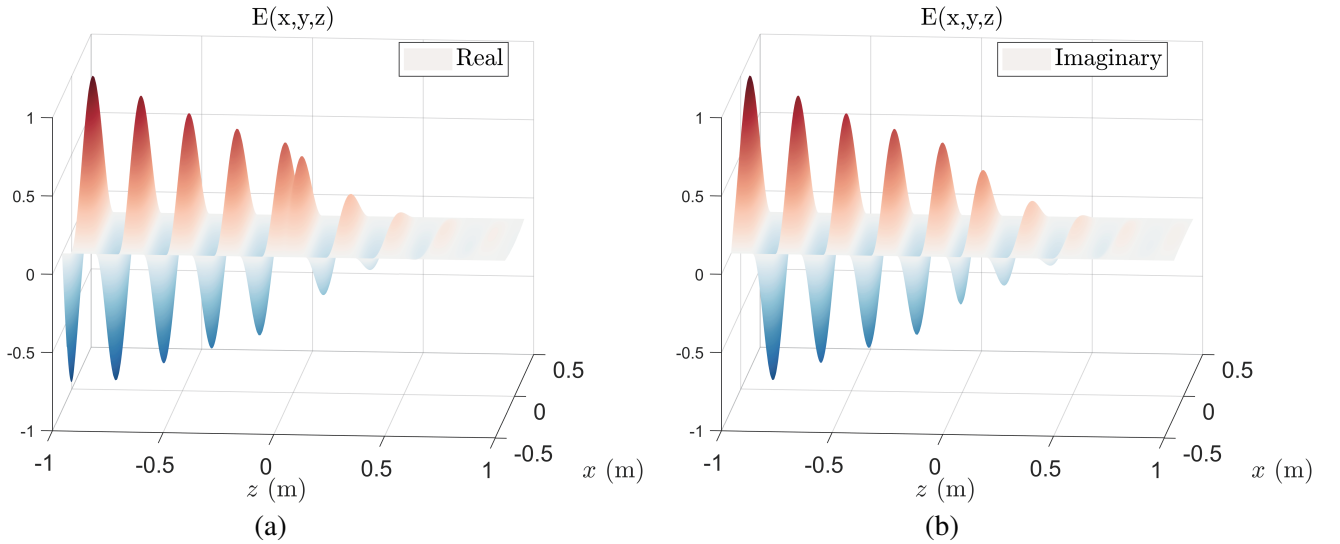


Figure 3. Numerically and analytically obtained 3D TE₁₀ electric field intensity $E(x, y, z)$. Figures (a) and (b) show the real and imaginary parts of the 3D electric field intensity, respectively.

RHM-LHM composites, which is important knowledge for related future work.

For electromagnetic fields in waveguides, it is common to present the field distribution patterns in the cross-section plane for different modes, i.e., different values of the integers m and n defined in Eq. (5). Such field distribution patterns are, however, unchanged by the grading in z -direction and can be found in textbooks on waveguides. They are therefore not included in the present paper, where we focus on graded material composites and their properties.

5. CONCLUSIONS

In the present paper, we have investigated the TE-wave propagation in a hollow waveguide filled with a lossy RHM-LHM composite with graded transition from a lossy RHM filling the left-hand half of the waveguide to the impedance-matched lossy LHM filling the right-hand half of the waveguide. The transition between the two media was graded along the z -direction, where the permittivity $\varepsilon(\omega, z)$ and permeability $\mu(\omega, z)$ are hyperbolic tangent functions of the z -coordinate. We have obtained exact analytical solutions to Maxwell's equations for lossy media and shown that the solutions for the field components are in line with the expected properties of RHM-LHM waveguide structures. Thereafter, a numerical study of the wave propagation over an impedance-matched graded RHM-LHM interface was performed, using COMSOL software. The numerical study shows an excellent agreement between the results obtained using numerical and analytical approach, respectively.

ACKNOWLEDGMENT

The work of M. D. was supported by the Swedish Research Council (VR) under project number 2018-05001.

REFERENCES

1. Wu, Q., J. P. Turpin, and D. H. Werner, "Integrated photonic systems based on transformation optics enabled gradient index devices," *Nature, Light: Science & Applications*, Vol. 1, e38, 1–6, Art No. 4700605, November 2012, doi: 10.1038/lisa.2012.38.

2. Zhang, N., W. X. Jiang, H. F. Ma, W. X. Tang, and T. J. Cui, "Compact high-performance lens antenna based on impedance-matching gradient-index metamaterials," *IEEE Transactions on Antennas and Propagation*, Vol. 67, 2, 1323–1328, February 2019, doi: 10.1109/TAP.2018.2880115.
3. Su, Y. and Z. N. Chen, "A flat dual-polarized transformation-optics beamsweeping luneburg lens antenna using PCB-stacked gradient index metamaterials," *IEEE Transactions on Antennas and Propagation*, Vol. 66, 10, 5088–5097, October 2018, doi: 10.1109/TAP.2018.2858209.
4. Luque-González, J. M., R. Halir, J. G. Wanguemert-Perez, J. de-Oliva-Rubio, J. H. Schmid, P. Cheben, Í. Molina-Fernandez, and A. Ortega-Monux, "An ultracompact GRIN-lens-based spot size converter using subwavelength grating metamaterials," *Laser Photonics Reviews*, Vol. 13, 19001724, 1–7, September 2019, doi: 10.1002/lpor.201900172.
5. Gauffillet, F., S. Marcellin, and E. Akmansoy, "Dielectric metamaterial-based gradient index lens in the terahertz frequency range," *IEEE Journal of Selected Topics in Quantum Electronics*, Vol. 23, 4, 1–5, Art No. 4700605, July/August 2017, doi: 10.1109/JSTQE.2016.2633825.
6. Salami, P. and L. Yousefi, "Far-field subwavelength imaging using phase gradient metasurfaces," *IEEE Journal of Lightwave Technology*, Vol. 37, 10, 2317–2323, March 2019, doi: 10.1109/JLT.2019.2902544.
7. Hajiahmadi, M. J., R. Faraji-Dana, and A. K. Skrivervik, "Far field superlensing inside biological media through a nanorod lens using spatiotemporal information," *Nature, Scientific Reports*, Vol. 11, 1–8, Art No. 19534, January 2021, doi: 10.1038/s41598-021-81091-0.
8. La Spada, L., T. M. McManus, A. Dyke, S. Haq, L. Zhang, Q. Cheng, and Y. Hao, "Surface wave cloak from graded refractive index nanocomposites," *Nature: Scientific Reports*, Vol. 6, 29363, July 2016, DOI: 10.1038/srep29363.
9. Hadi Badri, S., H. Rasooli Saghari, and H. Soofi, "Multimode waveguide crossing based on a square Maxwell's fisheye lens," *Applied Optics*, Vol. 58, 17, 4647–4653, June 2019, doi: 10.1364/AO.58.004647.
10. Fu, Y., Y. Xu, and H. Chen, "Applications of gradient index metamaterials in waveguides," *Nature, Scientific Reports*, Vol. 5, Art No. 18223, 1–6, December 2015, doi: 10.1038/srep18223.
11. El-Khozondar, H. J., R. J. El-Khozondar, A. Shama, K. Ahmed, and V. Dhasarathan, "Highly efficient solar energy conversion using graded-index metamaterial nanostructured waveguide," *Journal of Optical Communications*, eISSN 2191-6322, ISSN 0173-4911, February 2020, doi: 10.1515/joc-2019-0285.
12. Liu, Y. and S. Jian, "Tunable trapping and releasing light in graded graphene-silica metamaterial waveguide," *Optics Express*, Vol. 22, 24312–24321, October 2014, doi: 10.1364/OE.22.024312.
13. Hu, H.-F., D. Ji, X. Zeng, K. Liu, and Q. Gan, "Rainbow trapping in hyperbolic metamaterial waveguide," *Scientific Reports*, Vol. 3, 1249–1255, February 2013, doi: 10.1038/srep01249.
14. Yan, B., B. Yu, J. Xu, Y. Li, Z. Wang, Z. Wang, B. Yu, H. Ma, and C. Gong, "Customized meta-waveguide for phase and absorption," *Journal of Physics D: Applied Physics*, Vol. 54, 465102–465112, August 2021, doi: 10.1088/1361-6463/ac1466.
15. Weng, Q., Q. Lin, and H. Wu, "An efficient semianalytical modal analysis of rectangular waveguides containing metamaterials with graded inhomogeneity," *International Journal of Antennas and Propagation*, **2021**, 1–13, February 2021, doi: 10.1155/2021/6107378.
16. Berneschi, S., S. Soria, G. C. Righini, G. Alombert-Goget, A. Chiappini, A. Chiasera, Y. Jestin, M. Ferrari, S. Guddala, E. Moser, S. N. B. Bhaktha, B. Boulard, C. Duverger Arfuso, and S. Turrell, "Rare-earth-activated glass-ceramic waveguides," *Optical Materials*, Vol. 32, 1644–1647, May 2010, doi: 10.1016/j.optmat.2010.04.035.
17. Guddala, S., Y. Kawaguchi, F. Komissarenko, S. Kiriushechkina, A. Vakulenko, K. Chen, A. Alu, V. M. Menon, and A. B. Khanikaev, "All-optical nonreciprocity due to valley polarization pumping in transition metal dichalcogenides," *Nature Communications*, Vol. 12, 1–9, June 2021, doi: 10.1038/s41467-021-24138-0.
18. Estep, N. A., D. L. Sounas, J. Soric, and A. Alu, "Magnetic-free non-reciprocity and isolation based on parametrically modulated coupled-resonator loops," *Nature Physics*, Vol. 10, 923–927, November 2014, doi: 10.1038/nphys3134.

19. Keshavarz, S. and S. Dimitrios, “Topological transmission line metamaterials for microwave applications,” 194–196, August 2021, doi: 10.1109/Metamaterials52332.2021.9577096.
20. Keshavarz, S., A. Abdolali, A. Mohammadi, and R. Keshavarz, “Design and implementation of low loss and compact microstrip triplexer using CSRR loaded coupled lines,” *AEU — International Journal of Electronics and Communications*, Vol. 111, 152913, August 2019, doi: 10.1016/j.aeue.2019.152913.
21. Keshavarz, S., R. Keshavarz, and A. Abdipour, “Compact active duplexer based on CSRR and interdigital loaded microstrip coupled lines for LTE application,” *Progress In Electromagnetics Research C*, Vol. 109, 27–37, January 2021, doi: 10.2528/PIERC20112307.
22. Dalarsson, M., M. Norgren, T. Asenov, and N. Doncov, “Arbitrary loss factors in the wave propagation between RHM and LHM media with constant impedance throughout the structure,” *Progress In Electromagnetics Research*, Vol. 137, 527–538, March 2013, doi:10.2528/PIER13013004.
23. Dalarsson, M., “General theory of wave propagation through graded interfaces between positive- and negative refractive-index media,” *Physical Review A*, Vol. 96, 043848, October 2017, doi: PhysRevA.96.043848.
24. Dalarsson, M. and P. Tassin, “Analytical solution for wave propagation through a graded index interface between a right-handed and a left-handed material,” *Optics Express*, Vol. 17, 6747–6752, April 2009.
25. Dalarsson, M. and S. Nordebo, “TE-wave propagation in graded waveguide structures,” *OSA Continuum*, Vol. 3, 67–76, January 2020.